State-dependent forces in cold quantum gases

Christopher Billington

Submitted in total fulfilment of the requirements
of the degree of Doctor of Philosophy

Supervisory committee:
Prof Kristian Helmerson
Dr Lincoln Turner
Dr Russell Anderson

School of Physics and Astronomy
Monash University

August, 2016

rev: 19 (a3ca25bcaff8)
author: Chris Billington <chrisjbillington@gmail.com>
date: Thu Aug 04 16:01:52 2016 +1000
summary: Wordcount included in pdf at end

This page intentionally left blank

Contents


```
rev:     19 (a3ca25bcaff8)
author:  Chris Billington <chrisjbillington@gmail.com>
date:    Thu Aug 04 16:01:52 2016 +1000
summary: Wordcount included in pdf at end
```

This page intentionally left blank

Chapter 3

Quantum mechanics on a computer

This chapter comprises a summary of some of the methods used by cold atom physicists to compute numerical results pertaining to cold atom systems. Many a problem in quantum mechanics is not analytically solvable, especially when the real world of experimental physics rears its ugly head, violating theorists' assumptions of simplicitly left and right. In particular, atomic physics experiments are time-dependent, with each run of an experiment generally proceeding in stages. Lasers may turn on and off, magnetic fields may vary in magnitude and direction, RF pulses may be chirped [CITE LISA?] to reliably induce particular atomic transitions. Much of the numerical calculations performed by researchers in cold atom physics groups such as ours are accordingly of the time-dependent variety, and are fairly literal simulations of specific experiments that may be carried out in the lab.

To numerically simulate a quantum mechanical system, one must evolve a state vector in time according to the Schrödinger equation:

$$\frac{\mathrm{d}}{\mathrm{d}t}|\psi\rangle = \hat{H}|\psi\rangle \tag{3.1}$$

To do this on a computer, one must first decide which degrees of freedom are to be simulated. We necessarily neglect many degrees of freedom as a matter of course; which ones can be neglected is warranted by the specific situation and we do it so often we barely notice. For example, simulating a single component Bose–Einstein condensate entails neglecting the internal degrees of freedom of the atoms—as well as reducing the atom-light interaction to a simple potential such as an optical dipole trap or magnetic dipole interaction (neglecting the quantum degrees of freedom in the electromagnetic field). We may ignore one or more spatial degrees of freedom as well, say, if we are simulating an experiment in which the condensate is confined to two dimensions by way of a tight trapping potential in one direction [CITE AN EXAMPLE]. Or, when simulating laser cooling [SEE SECTION TODO], we may care very much about the electronic state of the atom, but treat its motional state classically. In these cases we are essentially imposing the assumption that the system will only occupy one state with respect to those degrees of freedom ignored (the condensate will remain in the ground state of the tight trap, the atoms will remain in one specific Zeeman sublevel), or we are assuming those degrees of freedom can be treated classically (the electromagnetic field is well described by classical electromagnetism, the atoms' motional state is described well by Newtonian mechanics).

Once the degrees of freedom are known, one must decide on a basis in which to represent them concretely. The basis often cannot be complete, since for many degrees of freedom this would require an infinite number of basis states—for example the electronic state of an atom contains a countably infinite number of states, whereas a spatial

```
rev:     19 (a3ca25bcaff8)
author:  Chris Billington <chrisjbillington@gmail.com>
date:    Thu Aug 04 16:01:52 2016 +1000
summary: Wordcount included in pdf at end
```

wavefunction in free space has an uncountable number of states (one for each position in R_3 [TODO BLACKBOARD BOLD]). For the internal state of an atom, therefore, we restrict ourselves to only the states we expect can become non-negligibly occupied, given the initial conditions and transitions involved. For example, at low temperature we can expect atoms to be almost completely in their electronic ground states, since energy gaps between ground and excited states are large compared to the atoms' thermal energy.[1]. We need only include the small number of excited states that might become occupied as a result of optical transitions present in the situation being simulated. This can still be a large number of states if one is studying Rydberg atoms or using ultrafast (and therefore broad-band) laser pulses, but is otherwise fairly small. Including both the D1 and D2 lines of Rubidium 87, with all hyperfine levels and Zeeman sublevels gives 32 states, for example (see section [TODO]).

[1] The D-line of rubidium 87 has an energy gap of [TODO], requiring a temperature of [TODO] or higher in order for the Boltzmann factor $e^{\frac{\Delta E}{kT}}$ describing the excited state population to be greater than 1×10^{-6}.

One the degrees of freedom and basis vectors have been chosen, the state vector is then represented on a computer as an array of complex numbers, giving the coefficients of each basis vector required to represent a particular state vector. Matrix elements of the Hamiltonian in the same basis must be calculated, and the Schrödinger equation can then be written:

$$\frac{\mathrm{d}}{\mathrm{d}t}|\psi\rangle = \hat{H}|\psi\rangle \tag{3.2}$$

3.1 Fourth order Runge–Kutta in an instantaneous local interaction picture

Consider the differential equation for the components of a state vector $|\psi(t)\rangle$ in a particular basis with basis vectors $|n\rangle$. This might simply be the Schrödinger equation, or perhaps some sort of nonlinear or other approximate, effective or phenomenological equation not corresponding to pure Hamiltonian evolution. Though they may have additional terms, such equations are generally of the form:

$$\frac{\mathrm{d}}{\mathrm{d}t}\langle n|\psi(t)\rangle = -\frac{i}{\hbar}\sum_m \langle n|\hat{H}(t)|m\rangle\,\langle m|\psi(t)\rangle\,, \tag{3.3}$$

where $\langle n|\hat{H}(t)|m\rangle$ are the matrix elements in that basis of the Hamiltonian $\hat{H}(t)$, which in general can be time dependent, or even a function of $|\psi(t)\rangle$, depending on the exact type of equation in use. If $\hat{H}(t)$ is almost diagonal in the $|n\rangle$ basis, then the solution to (3.3) is dominated by simple dynamical phase evolution, that is:

$$|\psi(t)\rangle \approx \sum_m e^{-\frac{i}{\hbar}E_m t}|m\rangle\,, \tag{3.4}$$

where E_m is the energy eigenvalue corresponding to the eigenstate $|m\rangle$.

A transformation into an interaction picture (IP) [1, p318] is commonly used to treat this part of the evolution analytically, before solving the remaining dynamics with further analytics or numerics. For numerical methods, integration in the interaction picture allows one to use larger integration timesteps, as one does not need to resolve the fast oscillations around the complex plane due to this dynamical phase.

Choosing an interaction picture typically involves diagonalising the time-independent part of a Hamiltonian, and then proceeding in the basis in which that time-independent part is diagonal. However, often one has a good reason to perform computations in a different basis, in which the time independent part of the Hamiltonian is only approximately diagonal,[2] and transforming between bases may be computationally expensive (involving large matrix-vector multiplications). Furthermore, the Hamiltonian may change sufficiently during the time interval being simulated that the original time-independent

[2] For example, a spatial basis which allows for partitioning the integration region over multiple nodes on a cluster or cores on a GPU.

rev: 19 (a3ca25bcaff8)
author: Chris Billington <chrisjbillington@gmail.com>
date: Thu Aug 04 16:01:52 2016 +1000
summary: Wordcount included in pdf at end

Hamiltonian no longer dominates the dynamics at later times. In both these cases it would still be useful to factor out the time-local oscillatory dynamics in whichever basis is being used, in order to avoid taking unreasonably small timesteps.

To that end, suppose we decompose $\hat{H}(t)$ into diagonal and non-diagonal (in the $|n\rangle$ basis) parts at each moment in time:

$$\hat{H}(t) = \hat{H}_{\text{diag}}(t) + \hat{H}_{\text{nondiag}}(t), \tag{3.5}$$

and use the diagonal part at a specific time $t = t'$ to define a time-independent Hamiltonian:

$$\hat{H}_0^{t'} = \hat{H}_{\text{diag}}(t'), \tag{3.6}$$

which is diagonal in the $|n\rangle$ basis. We can then use then use $\hat{H}_0^{t'}$ to define an interaction picture state vector:

$$|\psi_{\text{I}}^{t'}(t)\rangle = e^{\frac{i}{\hbar}(t-t')\hat{H}_0^{t'}} |\psi(t)\rangle\,, \tag{3.7}$$

which obeys the differential equation:

$$\frac{\mathrm{d}}{\mathrm{d}t}|\psi_{\text{I}}^{t'}(t)\rangle = e^{\frac{i}{\hbar}(t-t')\hat{H}_0^{t'}} \frac{\mathrm{d}}{\mathrm{d}t}|\psi(t)\rangle + \frac{i}{\hbar}\hat{H}_0^{t'}|\psi_{\text{I}}^{t'}(t)\rangle\,, \tag{3.8}$$

where:

$$|\psi(t)\rangle = e^{-\frac{i}{\hbar}(t-t')\hat{H}_0^{t'}} |\psi_{\text{I}}^{t'}(t)\rangle \tag{3.9}$$

is the original Schrödinger picture (SP) state vector.

This transformation is exact, no approximations or assumptions have been made. If indeed the dynamics of $|\psi(t)\rangle$ in the given basis are dominated by fast oscillating dynamical phases, that is, the diagonals of $\hat{H}_{\text{diag}}(t)$ are much greater than all matrix elements of $\hat{H}_{\text{nondiag}}(t)$ in the $|n\rangle$ basis, then solving the differential equation (3.8) for $|\psi_{\text{I}}^{t'}(t)\rangle$ should allow one to use larger integration timesteps than solving (3.3) directly. And if not, then it should do no harm other than the (small) computational costs of computing some extra scalar exponentials.

Equation (3.7) defines an *instantaneous* interaction picture, in that it depends on the dynamics at a specific time $t = t'$, and can be recomputed repeatedly throughout a computation in order to factor out the fast dynamical phase evolution even as the oscillation rates change over time. It is *local* in that $H_0^{t'}$ is diagonal in the $|n\rangle$ basis, which means that transformations between Schrödinger picture and interaction picture state vectors involves ordinary, elementwise exponentiation of vectors, rather than matrix products. Thus (3.7), (3.8) and (3.9) can be written componentwise as:

$$\langle n|\psi_{\text{I}}^{t'}(t)\rangle = e^{i(t-t')\omega_n^{t'}} \langle n|\psi(t)\rangle\,, \tag{3.10}$$

$$\frac{\mathrm{d}}{\mathrm{d}t}\langle n|\psi_{\text{I}}^{t'}(t)\rangle = e^{i(t-t')\omega_n^{t'}} \frac{\mathrm{d}}{\mathrm{d}t}\langle n|\psi(t)\rangle + i\omega_n^{t'}\langle n|\psi_{\text{I}}^{t'}(t)\rangle\,, \tag{3.11}$$

and:

$$\langle n|\psi(t)\rangle = e^{-i(t-t')\omega_n^{t'}} \langle n|\psi_{\text{I}}^{t'}(t)\rangle\,, \tag{3.12}$$

where we have defined:

$$\omega_n^{t'} = \frac{1}{\hbar}\langle n|\hat{H}_0^{t'}|n\rangle \tag{3.13}$$

```
rev:     19 (a3ca25bcaff8)
author:  Chris Billington <chrisjbillington@gmail.com>
date:    Thu Aug 04 16:01:52 2016 +1000
summary: Wordcount included in pdf at end
```

This is in contrast to fourth order Runge–Kutta in the interaction picture (RK4IP) [2], in which the interaction picture uses the Fourier basis and thus transforming to and from it involves fast Fourier transforms (FFTs). RK4IP was developed to augment computations in which FFTs were already in use for evaluating spatial derivatives, and so its use of FFTs imposes no additional cost. Nonetheless, an interaction picture based on the kinetic term of the Schrödinger equation (which is the term of the Hamiltonian that RK4IP takes as its time-independent part) may not be useful if that term does not dominate the Hamiltonian, as in the case of a Bose–Einstein condensate in the Thomas–Fermi limit. We compare the two methods below.

3.1.1 Algorithm

The *fourth order Runge–Kutta in an instantaneous local interaction picture* RK4ILIP algorithm is now obtained by using (3.7) to define a new interaction picture at the beginning of each fourth-order Runge–Kutta (RK4) integration timestep. The differential equation and initial conditions supplied to the algorithm are in the ordinary Schrödinger picture, and the interaction picture is used only within a timestep, with the Schrödinger picture state vector returned at the end of each timestep. Thus differential equations need not be modified compared to if ordinary RK4 were being used, and the only modification to calling code required is for a function to compute and return $\omega_n^{t'}$.

Being based on fourth order Runge–Kutta integration, this new method enjoys all the benefits of a workhorse method that is time-proven, and—as evidenced by its extremely widespread use—at a sweet-spot of ease of implementation, accuracy, and required computing power [3].

Below is the resulting algorithm for performing one integration timestep. It takes as input the time t_0 at the start of the timestep, the timestep size Δt, an array $\boldsymbol{\psi}_0$ containing the components $\{\langle n|\psi(t_0)\rangle\}$ of the state vector at time t_0, a function $F(t, \boldsymbol{\psi})$ which takes a time and (the components of) a state vector and returns an array containing the time derivative of each component, and a function $G(t, \boldsymbol{\psi})$ which takes the same inputs and returns an array containing the interaction picture oscillation frequency ω_n for each component at that time.

For example, for the case of the Gross–Pitaevskii equation [4] in the spatial basis $\psi(\boldsymbol{r}, t) = \langle \boldsymbol{r}|\psi(t)\rangle$, these would be:

$$F(t, \psi(\boldsymbol{r}, t)) = -\frac{i}{\hbar}\Big[\underbrace{-\frac{\hbar^2}{2m}\nabla^2}_{\hat{H}_{\text{nondiag}}} + \underbrace{V(\boldsymbol{r}, t) + g|\psi(\boldsymbol{r}, t)|^2}_{\hat{H}_{\text{diag}}}\Big]\psi(\boldsymbol{r}, t), \tag{3.14}$$

and

$$G(t, \psi(\boldsymbol{r}, t)) = \frac{1}{\hbar}\Big[\underbrace{V(\boldsymbol{r}, t) + g|\psi(\boldsymbol{r}, t)|^2}_{\hat{H}_{\text{diag}}}\Big]. \tag{3.15}$$

Note that each symbol in bold in the algorithm below denotes an array containing one element for each basis vector $|n\rangle$, subscripts denote the different stages of RK4, and all arithmetic operations between arrays are elementwise[3] The only opportunity for non-elementwise operations to occur is within F, which contains the details (via $\hat{H}_{\text{nondiag}}$) of any couplings between basis states for whatever system of equations is being solved, for example, using FFTs or finite differences to evaluate the Laplacian in (3.14).

[3] For example, the expression $\boldsymbol{a} \leftarrow e^{-i\omega\Delta t}\boldsymbol{b}$ indicates that for all n, $a_n \leftarrow e^{-i\omega_n\Delta t}b_n$, where a_n denotes the n^{th} element of $\boldsymbol{a}$ etc.

Algorithm 1 RK4ILIP

1: **function** RK4ILIP(t_0, Δt, $\boldsymbol{\psi}_0$, F)

```
rev:     19 (a3ca25bcaff8)
author:  Chris Billington <chrisjbillington@gmail.com>
date:    Thu Aug 04 16:01:52 2016 +1000
summary: Wordcount included in pdf at end
```

2: $\boldsymbol{f}_1 \leftarrow F(t_0, \boldsymbol{\psi}_0)$ ▷ First evaluation of Schrödinger picture DE
3: $\boldsymbol{\omega} \leftarrow G(t_0, \boldsymbol{\psi}_0)$ ▷ Oscillation frequencies: $\hbar\omega_n = \langle n|\hat{H}_{\text{diag}}(t_0)|n\rangle$
4: $\boldsymbol{k}_1 \leftarrow \boldsymbol{f}_1 + i\boldsymbol{\omega}\boldsymbol{\psi}_0$ ▷ Evaluate (3.11) with $t - t' = 0$
5: $\boldsymbol{\phi}_1 \leftarrow \boldsymbol{\psi}_0 + \boldsymbol{k}_1 \frac{\Delta t}{2}$ ▷ First RK4 estimate of IP state vector, at $t = t_0 + \frac{\Delta t}{2}$
6: $\boldsymbol{\psi}_1 \leftarrow e^{-i\boldsymbol{\omega}\frac{\Delta t}{2}}\boldsymbol{\phi}_1$ ▷ Convert first estimate back to SP with (3.12)
7: $\boldsymbol{f}_2 \leftarrow F(t_0 + \frac{\Delta t}{2}, \boldsymbol{\psi}_1)$ ▷ Second evaluation of Schrödinger picture DE
8: $\boldsymbol{k}_2 \leftarrow e^{i\boldsymbol{\omega}\frac{\Delta t}{2}}\boldsymbol{f}_2 + i\boldsymbol{\omega}\boldsymbol{\phi}_1$ ▷ Evaluate (3.11) with $t - t' = \frac{\Delta t}{2}$
9: $\boldsymbol{\phi}_2 \leftarrow \boldsymbol{\psi}_0 + \boldsymbol{k}_2 \frac{\Delta t}{2}$ ▷ Second RK4 estimate of IP state vector, at $t = t_0 + \frac{\Delta t}{2}$
10: $\boldsymbol{\psi}_2 \leftarrow e^{-i\boldsymbol{\omega}\frac{\Delta t}{2}}\boldsymbol{\phi}_2$ ▷ Convert second estimate back to SP with (3.12)
11: $\boldsymbol{f}_3 \leftarrow F(t_0 + \frac{\Delta t}{2}, \boldsymbol{\psi}_2)$ ▷ Third evaluation of Schrödinger picture DE
12: $\boldsymbol{k}_3 \leftarrow e^{i\boldsymbol{\omega}\frac{\Delta t}{2}}\boldsymbol{f}_3 + i\boldsymbol{\omega}\boldsymbol{\phi}_2$ ▷ Evaluate (3.11) with $t - t' = \frac{\Delta t}{2}$
13: $\boldsymbol{\phi}_3 \leftarrow \boldsymbol{\psi}_0 + \boldsymbol{k}_3 \Delta t$ ▷ Third RK4 estimate of IP state vector, at $t = t_0 + \Delta t$
14: $\boldsymbol{\psi}_3 \leftarrow e^{-i\boldsymbol{\omega}\Delta t}\boldsymbol{\phi}_3$ ▷ Convert third estimate back to SP with (3.12)
15: $\boldsymbol{f}_4 \leftarrow F(t_0 + \Delta t, \boldsymbol{\psi}_3)$ ▷ Fourth evaluation of Schrödinger picture DE
16: $\boldsymbol{k}_4 \leftarrow e^{i\boldsymbol{\omega}\Delta t}\boldsymbol{f}_4 + i\boldsymbol{\omega}\boldsymbol{\phi}_3$ ▷ Evaluate (3.11) with $t - t' = \Delta t$
17: $\boldsymbol{\phi}_4 \leftarrow \boldsymbol{\psi}_0 + \frac{\Delta t}{6}(\boldsymbol{k}_1 + 2\boldsymbol{k}_2 + 2\boldsymbol{k}_3 + \boldsymbol{k}_4)$ ▷ Fourth RK4 estimate, at $t = t_0 + \Delta t$
18: $\boldsymbol{\psi}_4 \leftarrow e^{-i\boldsymbol{\omega}\Delta t}\boldsymbol{\phi}_4$ ▷ Convert fourth estimate back to SP with (3.12)
19: **return** $\boldsymbol{\psi}_4$ ▷ Return the computed SP state vector at $t = t_0 + \Delta t$
20: **end function**

Note on imaginary time evolution

When RK4ILIP is used for imaginary time evolution (ITE) [5], the oscillation frequencies $\boldsymbol{\omega}$ may have a large imaginary part. If the initial guess is different enough from the ground state, then the exponentials in (3.10), (3.11) and (3.12) may result in numerical overflow. To prevent this, one can define a clipped copy of $\boldsymbol{\omega}$,

$$\boldsymbol{\omega}_{\text{clipped}} = \text{Re}(\boldsymbol{\omega}) + i\begin{cases} -\frac{\log X}{\Delta t} & \text{Im}(\boldsymbol{\omega})\Delta t < -\log X \\ \text{Im}(\boldsymbol{\omega}) & -\log X \le \text{Im}(\boldsymbol{\omega})\Delta t \le \log X \\ \frac{\log X}{\Delta t} & \text{Im}(\boldsymbol{\omega})\Delta t > \log X \end{cases}, \tag{3.16}$$

where X is very large but less than the largest representable floating-point number, and use $\boldsymbol{\omega}_{\text{clipped}}$ in the exponents instead. In the below results I used RK4ILIP with ITE to smooth initial states of a Bose–Einstein condensate after a phase printing, and performed clipping with [4] $\log X = 400$.

This clipped version of $\boldsymbol{\omega}$ should be used in all exponents in the above algorithm, but only in exponents—not in the second term of (3.11). If it is used everywhere then all we have done is chosen a different (less useful) interaction picture, and the algorithm will still overflow. By clipping only the exponents, we produce temporarily "incorrect" evolution[5], limiting the change in magnitude of each component of the state vector to a factor of X per step (remembering that X is very large). This continues for the few steps that it takes ITE to get all components of the state vector to within a factor of X of the ground state, after which no clipping is necessary and convergence to the ground state proceeds as normal, subject to the ordinary limitations on which timesteps may be used with ITE.

[4] 400 being about half the largest (base e) exponent representable in double-precision floating point.

[5] Of no concern since we are using ITE as a relaxation method, and are not interested in intermediate states. Only the final state's correctness concerns us.

3.1.2 Domain of improvement over other methods

For simulations in the spatial basis, RK4ILIP treats the spatially local part of the Hamiltonian analytically to first order, and hence can handle larger potentials than ordinary RK4.

```
rev:     19 (a3ca25bcaff8)
author:  Chris Billington <chrisjbillington@gmail.com>
date:    Thu Aug 04 16:01:52 2016 +1000
summary: Wordcount included in pdf at end
```

However, since a global energy offset can be applied to any potential with no physically meaningful change in the results, ordinary RK4 can also handle large potentials — if they are large due a a large constant term which can simply be subtracted off.

So RK4ILIP is only of benefit in the case of large *spatial variations* in the potential. Only one constant can be subtracted off potentials without changing the physics — subtracting a spatially varying potential would require modification of the differential equation in the manner of a gauge transformation in order to leave the system physically unchanged[6].

[6] Though a numerical solution based on analytically gauging away potentials at each timestep might be equally as fruitful as RK4ILIP.

However that's not quite all: large spatial variation in potentials often comes with the prospect of the potential energy turning into kinetic energy, in which case RK4ILIP is also of little benefit, since in order to resolve the dynamical phase due to the large kinetic term, it would require timesteps just as small as those which ordinary RK4 would need to resolve the dynamical phase evolution from the large potential term.

This leaves RK4ILIP with an advantage only in the case of large spatial variations in the potential that do not lead to equally large kinetic energies. Hence the examples I show in the next section are ones in which the condensate is trapped in a steep potential well—the trap walls are high and hence involve large potentials compared to the interior, but do not lead to large kinetic energies because the condensate is trapped close to its ground state.

The Fourier split-step (FSS) method [6] (see section [TODO]) also models dynamical phases due to the potential analytically to low order. As such it is also quite capable of modeling large potentials. However, it requires that all operators be diagonal in either the spatial basis or the Fourier basis [6]. Therefore BECs in rotating frames, due to the Hamiltonian containing an angular momentum operator, are not amenable to simulation with FSS[7].

[7] Split-step with more than these two bases is however possible in other schemes such as the finite element discrete variable representation [7]—each operator can be diagonalised and exponentiated locally in each element and applied as a (relatively small) matrix multiplication rather than using FFTs.

This use of FFTs in both the FSS and RK4IP methods necessarily imposes periodic boundary conditions on a simulation, which may not be desirable. By contrast, if different boundary conditions are desired, finite differences instead of FFTs can be used to evaluate spatial derivatives in the RK4 and RK4ILIP methods, so long as a sufficiently high-order finite difference scheme is used so as not to unacceptably impact accuracy.

Along with the ability to impose arbitrary boundary conditions, finite differences require only local data, that is, only points spatially close to the point being considered need be known in order to evaluate derivatives there. This makes finite differences amenable to simulation on cluster computers [8, p100], with only a small number of points (depending on the order of the scheme) needing to be exchanged at node-boundaries each step. By contrast, FFT based derivatives require data from the entire spatial region. Whilst this can still be parallelised on a GPU, where all the data is available, it cannot be done on a cluster without large amounts of data transfer between nodes [9]. Thus, RK4 and RK4ILIP, being implementable with finite difference schemes, are considerably friendlier to cluster computing.

Table3.1 summarises the capabilities of the four methods considered in the following results section. RK4ILIP is the only method capable of modelling a large spatial variation in the potential term whilst being locally parallelisable, and supporting arbitrary operators and boundary conditions.

3.1.3 Results

Here I compare four numerical methods: Fourier split-step (FSS), fourth order Runge–Kutta in the interaction picture (RK4IP), ordinary fourth order Runge–Kutta (RK4), and my new method — fourth order Runge–Kutta in an instananeous local interaction picture (RK4ILIP).

The example chosen is a 2D simulation of a turbulent Bose–Einstein condensate, in both a rotating and nonrotating frame. For the nonrotating frame the differential

```
rev:     19 (a3ca25bcaff8)
author:  Chris Billington <chrisjbillington@gmail.com>
date:    Thu Aug 04 16:01:52 2016 +1000
summary: Wordcount included in pdf at end
```

Method	RK4	RK4IP	RK4ILIP	FSS
Error	$\mathcal{O}(\Delta t^4)$	$\mathcal{O}(\Delta t^4)$	$\mathcal{O}(\Delta t^4)$	$\mathcal{O}(\Delta t^2)$
FFTs per step	4	4	4	2
Large ΔV	No	No	Yes	Yes
Large kinetic term	No	Yes	No	Yes
Arbitrary operators	Yes	Yes†	Yes	No
Locally parallelisable	Yes	No	Yes	No
Arbitrary boundary conditions	Yes	No	Yes	No

Table 3.1: Advantages and disadvantages of four timestepping methods for simulating Bose–Einstein condensates. *Large* ΔV refers to whether the method can simulate potentials that vary throughout space by an amount larger than the energy scale $2\pi\hbar/\Delta t$ associated with the simulation timestep Δt. *Arbitrary operators* refers to whether the method permits operators that are not diagonal in either the spatial or Fourier basis, such as angular momentum operators. *Locally parallelisable* means the method can be formulated so as to use only spatially nearby points in evaluating operators, and thus is amenable to parallelisation by splitting the simulation over multiple cores in the spatial basis. † Whilst one can include arbitrary operators within the RK4IP method, only operators diagonal in Fourier space can be analytically treated the way RK4IP treats the kinetic term, and so there is no advantage for these terms over ordinary RK4.

```
rev:     19 (a3ca25bcaff8)
author:  Chris Billington <chrisjbillington@gmail.com>
date:    Thu Aug 04 16:01:52 2016 +1000
summary: Wordcount included in pdf at end
```

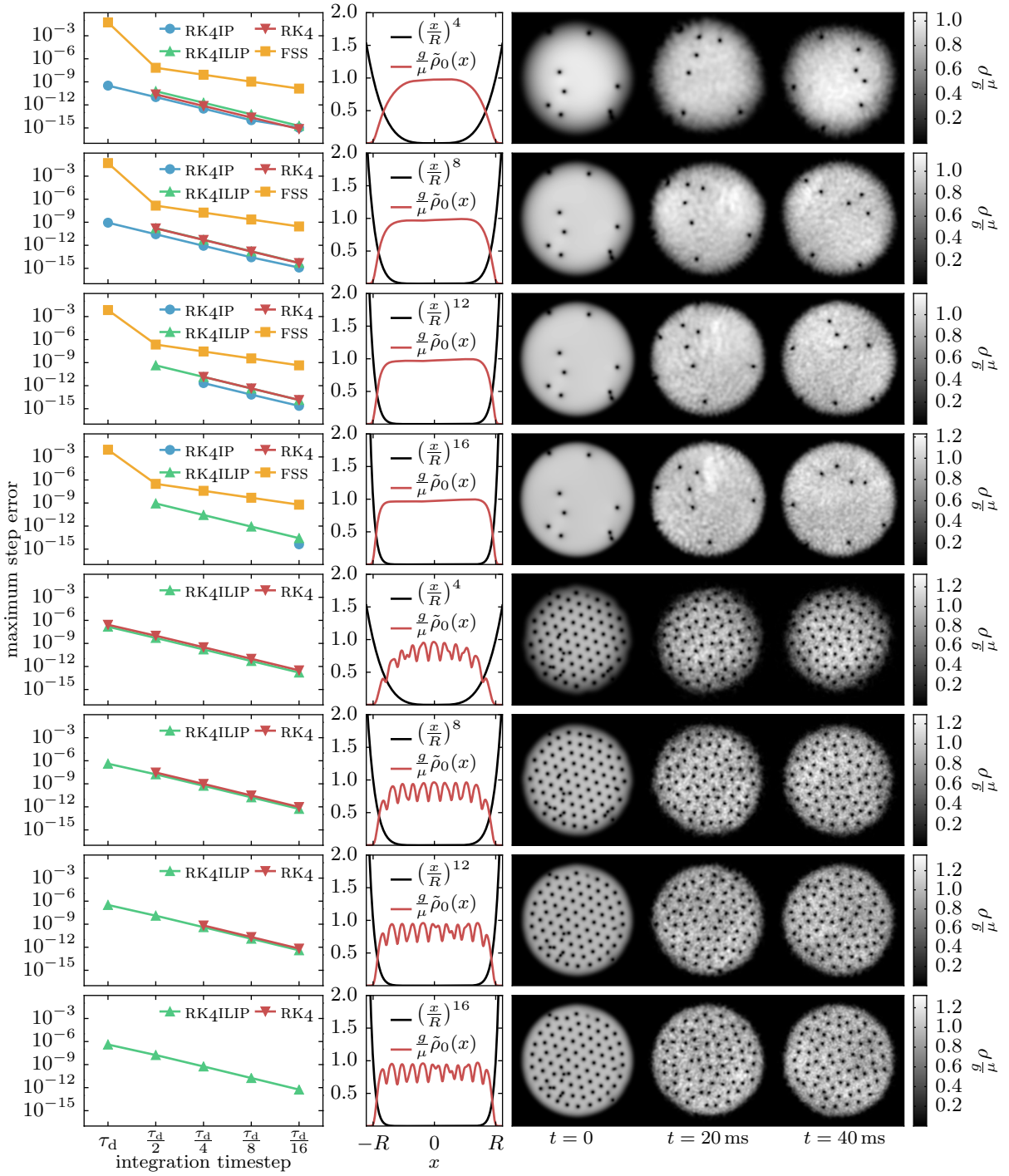

Figure 3.1: Results of simulations to compare RL4ILIP to other timestepping methods. Top four rows: Nonrotating frame simulations with four different radial power-law potentials. Bottom four rows: Rotating frame simulations with same four potentials. Left column: maximum per-step error $\int |\psi - \tilde{\psi}|^2 \,\mathrm{d}\boldsymbol{r} / \int |\tilde{\psi}|^2 \,\mathrm{d}\boldsymbol{r}$ of fourth order Runge–Kutta (RK4), its interaction picture variants (RK4IP and RK4ILIP) and Fourier split-step (FSS) as a function of timestep. Solutions were checked every 100 timesteps against a comparison solution $\tilde{\psi}$ computed using half sized steps for RK4 methods, and quarter sized steps for FSS. Simulations encountering numerical overflow not plotted. Centre column: potential (black) and average density $\tilde{\rho}_0$ of the initial state (red) over a slice of width $R/5$ in the y direction. Right column: Density of solution at initial, intermediate and final times for each configuration simulated (taken from RK4ILIP results). RK4ILIP is the only method usable in rotating frames and not encountering overflow in the steeper traps for the timesteps considered.

```
rev:     19 (a3ca25bcaff8)
author:  Chris Billington <chrisjbillington@gmail.com>
date:    Thu Aug 04 16:01:52 2016 +1000
summary: Wordcount included in pdf at end
```

equation simulated was equation (3.14), and for the rotating frame the same equation was with an additional two terms added to the Hamiltonian:

$$\hat{H}_{\text{rot}} + \hat{H}_{\text{comp}} = -\boldsymbol{\Omega} \cdot \hat{\boldsymbol{L}} + \frac{1}{2}\hbar m^2 \Omega^2 r^2 \tag{3.17}$$

$$= i\hbar\Omega\left(x\frac{\partial}{\partial y} - y\frac{\partial}{\partial x}\right) + \frac{1}{2}\hbar m^2 \Omega^2 r^2. \tag{3.18}$$

The addition of the first term transforms the original Hamiltonian into a frame rotating at angular frequency Ω in the (x, y) plane, and is equivalent to the the Coriolis and centrifugal forces that appear in rotating frames in classical mechanics [10]. The second term is a harmonic potential that exactly compensates for the centrifugal part of this force. In this way the only potential in the rotating frame is the applied trapping potential, and the only effect of the rotating frame is to add the Coriolis force.

Four trapping potentials were used, all radial power laws with different powers. These examples were chosen to demonstrate the specific situation in which RK4ILIP provides a benefit over the other methods for spatial Schrödinger-like equations, as discussed above.

The results of 120 simulation runs are shown in Figure 3.1. Each simulation was of a ^{87}Rb condensate in the $|F = 2, m_F = 2\rangle$ state, in which the two-body s-wave scattering length is $a = 98.98$ Bohr radii [11]. The simulation region was 20 μm in the x and y directions, and the Thomas–Fermi radius of the condensate was $R = 9$ μm. The chemical potential was $\mu = 2\pi\hbar \times 1.91$ kHz, which is equivalent to a maximum Thomas–Fermi density $\rho_{\text{max}} = 2.5 \times 10^{14}\,\text{cm}^{-3}$ and a healing length $\xi = 1.1$ μm. There were 256 simulation grid points in each spatial dimension, which is 14 points per healing length.

Four different potentials were used, all of the form $V(r) = \mu\,(r/R)^\alpha$ with $\alpha = 4, 8, 12, 16$. For the rotating frame simulations, the rotation frequency was $\Omega = 2\pi \times 148$ Hz. This is 89% of the effective harmonic trap frequency, defined as the frequency of a harmonic trap that would have the same Thomas–Fermi radius given the same chemical potential.

All ground states were determined using successive over-relaxation (See section [TODO]) with sixth-order finite differences for spatial derivatives. For the nonrotating simulations, convergence was reached with $\Delta\mu/\mu < 1 \times 10^{-13}$, with:

$$\Delta\mu = \sqrt{\frac{\langle\psi|(\hat{H} - \mu)^2|\psi\rangle}{\langle\psi|\psi\rangle}}, \tag{3.19}$$

where $\hat{H}$ is the nonlinear Hamiltonian and $\langle \boldsymbol{r}|\psi\rangle$ is the condensate wavefunction, which does not have unit norm. For the rotating frame simulations the ground states converged to $\Delta\mu/\mu \approx 9\times10^{-7}, 2\times10^{-6}, 3\times10^{-6}$ and 2×10^{-6} for $\alpha = 16, 12, 8$, and 4 respectively.

After each ground state was found, it was multiplied by a spatially varying phase factor corresponding to the phase pattern of a number of randomly positioned vortices:

$$\psi_{\text{vortices}}(x, y) = \psi_{\text{groundstate}}(x, y) \prod_{n=1}^{N} e^{\pm_n i \arctan2(y-y_n, x-x_n)} \tag{3.20}$$

where arctan2 is the two-argument arctan function,[8] $N = 30$, $\pm_n$ is a randomly chosen sign, and (x_n, y_n) are vortex positions randomly drawn from a Gaussian distribution centred on $(0, 0)$ with standard deviation equal to the Thomas–Fermi radius R. The same seed was used for the pseudorandom number generator in each simulation run, and so the vortex positions were identical in each simulation run.

[8] Defined as the principle value of the argument of the complex number $x + iy$: $\arctan2(y, x) = \text{Arg}(x + iy)$.

After vortex phase imprinting, the wavefunctions were evolved in imaginary time [5]. For the nonrotating frame simulations, imaginary time evolution was performed for a time interval equal to the chemical potential timescale $\tau_\mu = 2\pi\hbar/\mu$, and for the rotating

rev: 19 (a3ca25bcaff8)
author: Chris Billington <chrisjbillington@gmail.com>
date: Thu Aug 04 16:01:52 2016 +1000
summary: Wordcount included in pdf at end

frame simulations, for $\tau_\mu/10$. This was done to smooth out the condensate density in the vicinity of vortices, producing the correct density profile for vortex cores. However, since imaginary time evolution decreases the energy of the state indiscriminately, it also had the side effect of causing vortices of opposite sign to move closer together and annihilate. This decreased the number of vortices, and is the reason the smoothing step in the rotating frame simulations was cut short to $\tau_\mu/10$, as otherwise all vortices had time to annihilate with one of the lattice vortices. A vortex pair in the process of annihilating is visible in Figure 3.1 as a partially filled hole in the initial density profile near the top of the condensate in the $\alpha = 4$, 12, and 16 rotating frame simulations.[9]

[9] The initial states for the four different potentials are not identical, so by chance the corresponding vortex in the $\alpha = 8$ case was not close enough to a lattice vortex to annihilate.

The smoothed, vortex imprinted states were then evolved in time for 40 ms. For each simulation, five different timesteps were used: $\Delta t = \tau_d, \tau_d/2, \tau_d/4, \tau_d/8, \tau_d/16$, where $\tau_d = m\Delta x^2/\pi\hbar \approx 2.68\,\mu s$ is the dispersion timescale associated with the grid spacing Δx, defined as the time taken to move one gridpoint at the phase velocity of the Nyquist mode.

For the nonrotating frame simulations, spatial derivatives for the RK4 and RK4ILIP methods were determined using the Fourier method [see section TODO]. This was to ensure a fair comparison with the other two methods, which necessarily use Fourier transforms to perform computations pertaining due to the kinetic term.

For the rotating frame simulations, sixth-order finite differences with zero boundary conditions were used instead for the kinetic terms of the RK4 and RK4ILIP methods, which were the only two methods used for those simulations (due to the other methods being incompatible with the angular momentum operator required for a rotating frame). This choice was fairly arbitrary, but did allow the condensate to be closer to the boundary than is otherwise possible with the periodic boundary conditions imposed by use of the Fourier method for spatial derivatives. This is because the rotating frame Hamiltonian is not periodic in space, and so its discontinuity at the boundary can be a problem if the wavefunction is not sufficiently small there.

As shown in Figure 3.1, all methods tested generally worked well until they didn't work at all, with the per-step error of RK4-based methods being either small and broadly the same as the other RK4-based methods, or growing rapidly to the point of numerical overflow (shown as missing datapoints). The break down of FSS was less dramatic, though it too had a clear jump in its per-step error for larger timesteps. Comparing methods therefore came down to mostly whether or not a simulation experienced numerical overflow during the time interval being simulated.

The main result was that RK4ILIP and FSS remained accurate over the widest range of timesteps and trap steepnesses, with RK4 and RK4IP requiring ever smaller timesteps in order to not overflow as the trap steepness increased.

For the rotating frame simulations, which were only amenable to the RK4 and RK4ILIP methods, the same pattern was observed, with RK4 only working at smaller timesteps as the trap steepness was increased, and ultimately diverging for all timesteps tested at the maximum trap steepness. By contrast, RK4ILIP remained accurate over the entire range of timesteps at the maximum trap steepness.

3.1.4 Discussion

As mentioned, RK4ILIP is mostly useful for continuum quantum mechanics only when there are large spatial differences in the potential, which cannot give rise to equally large kinetic energies[10]. Furthermore, the advantage that RK4ILIP has over other methods with that same property is that it is does not require a particular form of Hamiltonian or a particular method of evaluating spatial derivatives. The former means is is applicable in rotating frames or to situations with unusual Hamiltonians, and the latter means is can be used with finite differences or FEDVR [7] and thus is amenable to parallelisation on a cluster computer.

[10] This is essentially due to such a situation violating the condition we laid out at the beginning of this section — that the simulation basis must be nearly an eigenbasis of the total Hamiltonian.

```
rev:     19 (a3ca25bcaff8)
author:  Chris Billington <chrisjbillington@gmail.com>
date:    Thu Aug 04 16:01:52 2016 +1000
summary: Wordcount included in pdf at end
```

The ability to model large spatial variations in the potential provides only a narrow domain of increased usefulness over other methods. If a large kinetic energy results from the large potential, then the method requires just as small timesteps as any other. And if the large potential is supposed to approximate an an infinite well, then an actual infinite well may be modelled using zero boundary conditions, negating the need for something like RK4ILIP. However, when potential wells are steep, but not infinitely steep, here RK4ILIP provides a benefit. The only other model that can handle these large potentials—Fourier split-step—has the disadvantage that it cannot deal with arbitrary operators such as those arising from a rotating frame, and is not parallelisable with local data. The benefits of parallelisability are obvious, and the above results demonstrate RK4ILIP's advantage at simulating BECs in tight traps and rotating frames.

For systems with discrete degrees of freedom, RK4ILIP may be useful in the case where an approximate diagonalisation of the Hamiltonian is analytically known, and when the Hamiltonian's eigenvalues vary considerably in time (making a single interaction picture insufficient to factor out dynamical phases throughout the entire simulation). In this situation an analytic transformation into the diagonal basis can be performed at each timestep (or the differential equation analytically re-cast in that basis in the first place), and RK4ILIP can be used to factor out the time-varying dynamical phase evolution at each timestep. An example may be an atom with a magnetic moment in a time-varying magnetic field which varies over orders of magnitude. The transformation into the spin basis in the direction of the magnetic field can be analytically performed, and if the field varies by orders of magnitude, so do the eigenvalues of the Hamiltonian. Although the eigenvalues in this case and other similar cases can be computed analytically too, unless all time dependence of the Hamiltonian is known in advance of the simulation, it would be difficult to incorporate this into a re-casting of the differential equation in a time-dependent interaction picture. RK4ILIP may be useful in these cases to automate this process and evolve the system in the appropriate interaction picture at each timestep.

rev: 19 (a3ca25bcaff8)
author: Chris Billington <chrisjbillington@gmail.com>
date: Thu Aug 04 16:01:52 2016 +1000
summary: Wordcount included in pdf at end

This page intentionally left blank

References

[1] J. J. Sakurai. *Modern quantum mechanics*. Addison-Wesley Pub. Co, Reading, Mass (1994). [p 4]

[2] Benjamin M. Caradoc Davies. *Vortex dynamics in Bose–Einstein condensates*. PhD thesis, University of Otago, Dunedin, New Zealand (2000). [p 6]

[3] W.H. Press. *The art of scientific computing*. Cambridge University Press (1992). [p 6]

[4] C.J. Pethick and H. Smith. *Bose–Einstein condensation in dilute gases*. Cambridge University Press (2002). [p 6]

[5] M. L. Chiofalo, S. Succi, and M. P. Tosi. *Ground state of trapped interacting Bose–Einstein condensates by an explicit imaginary-time algorithm*. Phys. Rev. E **62**, 7438 (2000). DOI: 10.1103/PhysRevE.62.7438. [pp 7 and 11]

[6] G.M. Muslu and H.A. Erbay. *Higher-order split-step Fourier schemes for the generalized nonlinear Schrödinger equation*. Mathematics and Computers in Simulation **7**, 581 (2005). DOI: 10.1016/j.matcom.2004.08.002. [p 8]

[7] Barry I. Schneider, Lee A. Collins, and S. X. Hu. *Parallel solver for the time-dependent linear and nonlinear Schrödinger equation*. Phys. Rev. E **73**, 036708 (2006). DOI: 10.1103/PhysRevE.73.036708. [pp 8 and 12]

[8] M.A. Heroux, P. Raghavan, and H.D. Simon. *Parallel processing for scientific computing*. Society for Industrial and Applied Mathematics, Philadelphia, PA (2006). [p 8]

[9] Anshul Gupta and Vipin Kumar. *The scalability of FFT on parallel computers*. IEEE Transactions on Parallel and Distributed Systems **4**, 922 (1993). [p 8]

[10] P. Gulshani and D. J. Rowe. *Quantum mechanics in rotating frames. I. The impossibility of rigid flow*. Canadian Journal of Physics **56**, 468 (1978). DOI: 10.1139/p78-060. [p 11]

[11] E. G. M. van Kempen, S. J. J. M. F. Kokkelmans, D. J. Heinzen, and B. J. Verhaar. *Interisotope determination of ultracold rubidium interactions from three high-precision experiments*. Phys. Rev. Lett. **88**, 093201 (2002). DOI: 10.1103/PhysRevLett.88.093201. [p 11]


```
rev:     19 (a3ca25bcaff8)
author:  Chris Billington <chrisjbillington@gmail.com>
date:    Thu Aug 04 16:01:52 2016 +1000
summary: Wordcount included in pdf at end
```

This page intentionally left blank

Word count

```
Total
Words in text: 5944
Words in headers: 155
Words outside text (captions, etc.): 718
Number of headers: 38
Number of floats/tables/figures: 6
Number of math inlines: 184
Number of math displayed: 32
Files: 9
Subcounts:
  text+headers+captions (#headers/#floats/#inlines/#displayed)
  89+48+0 (11/0/1/0) File(s) total: atomic_physics.tex
  106+19+0 (5/0/0/0) File(s) total: experiment.tex
  50+0+0 (0/0/0/0) File(s) total: front_matter.tex
  1355+19+65 (3/2/39/13) File(s) total: hidden_variables.tex
  88+1+0 (1/0/0/0) File(s) total: introduction.tex
  4104+29+535 (7/2/142/19) File(s) total: numerics.tex
  64+10+0 (5/0/0/0) File(s) total: software.tex
  52+16+118 (3/2/2/0) File(s) total: velocimetry.tex
  36+13+0 (3/0/0/0) File(s) total: wave_mixing.tex
```

```
rev:     19 (a3ca25bcaff8)
author:  Chris Billington <chrisjbillington@gmail.com>
date:    Thu Aug 04 16:01:52 2016 +1000
summary: Wordcount included in pdf at end
```